arXiv:2403.15090v1 [cond-mat.str-el] 22 Mar 2024

Symmetry, Superposition and Fragmentation in Classical Spin Liquids: A General Framework and Applications to Square Kagome Magnets

K.B. Yogendra, Suman Karmakar, and Tanmoy Das
Department of Physics, Indian Institute of Science, Bangalore 560012, India

Classical magnets offer glimpses of quantum-like features like spin liquids, and fractionalization, promising an analogous construction of superposition and projective symmetry in classical field theory. While models based on system-specific spin-ice or soft-spin rules exist, a formal theory for general classical magnets remains elusive. Here, we introduce a *mutatis mutandis* symmetry group construction built from a vector field in a plaquette of classical spins, demonstrating how classical spins superpose in irreducible representations (irreps) of the symmetry group. The corresponding probability amplitudes serve as order parameters and local spins as fragmented excitations. The formalism offers a many-body vector field representation of diverse ground states, including spin liquids and fragmented phases described as degenerate ensembles of irreps. We apply the theory specifically to a frustrated square Kagome lattice, where spin-ice or soft spin rules are inapt, to describe spin liquids and fragmented phases, all validated through irreps ensembles and unbiased Monte Carlo simulation. Our work sheds light on previously unknown aspects of spin-liquid phases and fragmentation and broadens their applications to other branches of field theory.

Classical spin models can potentially capture exotic phenomena like spin liquid [1–6], spin ice [7–9], and fragmentation [2, 10–13], order by disorder [14–18], prethermal discrete time crystals[19], and exciting progress lies in designing novel frameworks that mimic quantum principles [6, 20–26]. One approach, commonly known as the spin-ice rule, utilizes a class of Hamiltonians expressed in a quadratic form of total spins within a unit cell, enabling the depiction of a spin-zero degenerate manifold for spin ice/liquid ground states [2, 6, 11, 22, 23]. On the other hand, within a soft-spin approximation, analyzing the eigenenergy spectrum in the Fourier space of extended spin states enables convenient exploration of global symmetry and topology of many-body spins, but local spin conservation is sacrificed here[22–26]. Conversely, real-space studies of local spins offer complementary advantages, accommodating local constraints, local symmetries, order parameters, and monopole textures.[4, 6, 11, 27, 28] Both approaches intertwine in capturing salient features of spin liquids: dispersionless momentum-space energy mirrors extensive real-space spin degeneracy. Furthermore, singular pinch-point features in the correlation function[4, 6, 11, 28, 29] corresponds to gapless points with singular wavefunction in excitation energy dispersion.[24, 25] Another approach utilizes traditional Landau's coarse-grained magnetization fields, with or without enforcing local constraints, which can be fragmented into components exhibiting distinct correlation properties [10, 11, 30, 31].

Extensive research on these paradigms has explored frustrated lattices like pyrochlore [6, 28, 32–34], triangular [35–37], and Kagome [29, 38, 39], with earlier work focussing on other lattices[4, 15, 18, 40]. Recent excitement surrounds the square Kagome lattice (Fig. 1), spurred by experimental hints of spin liquid phases [41–43] and supported by theoretical investigations using variants of the Heisenberg model[44–48]. There are, however, indications of finite Dzyaloshinskii-Moriya (DM) interaction in these materials [41–43] which cannot be adequately captured within the spin-ice or soft-spin models. Moreover, a square Kagome lattice, boasting several sublattices, presents a superior setting with an enlarged degenerate manifold and increased fragmentation possibilities that remained unexplored. We study a classical spin model with XXZ and DM interactions on a two-dimensional square-Kagome lattice. Our approach transcends a prior approach[28, 29], which initiates by defining the symmetry group of the classical spin vector within a translationally invariant plaquette. Consequently, irreps of the symmetry group form the local basis states, enabling the plaquette field to superpose between them, and local spins emerge as their fragmented entities. Expansion parameters, behaving as Landau-like order parameters, transform, however, under 'discrete' spatial rotations. Interestingly, the order parameters serve as spin's 'probability amplitudes' and 'occupation densities' to irreps state and energy levels. Notably, the properties indeed echo quantum-like constructions. Through unbiased classical Monte Carlo simulations, we observe that DM interactions promote uniform or staggered ordering of irreps containing vortex or anti-vortex, while CSL states emerge near their critical phase boundaries. In the CSL phase, local spins remain either fully disordered if the ground state consists of a randomly distributed irrep ensemble or are fragmented into extended and point-like entities if the ground state scrambles order and disorder irreps. Additionally, the spin-spin correlation function is analyzed in each phase to distinguish between collective and fragmented excitations with Bragg-like peaks in the order phase, coexisting with pinch-point excitations in the liquid phases.

Mathematical foundation: Analogous to the product

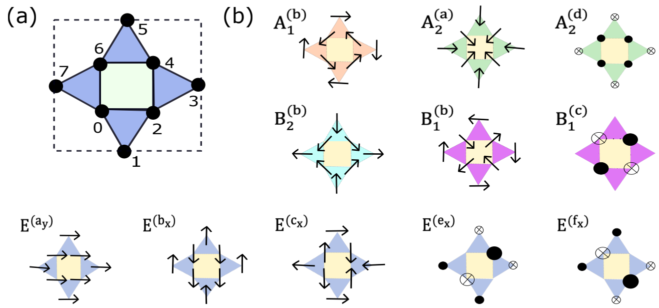

FIG. 1. (a) A plaquette of a 2D square-Kagome lattice, belonging to the D_4 group, is shown with sublattices enumerated as $i = 0 - 7$. (b) Among five irreps with different multiplets, we show a few representative irreps here, while others are shown in *SM*. Each irrep consists of either $S_i^{\perp}$ (horizontal arrow) or S_i^z (open and filled dots for up and down spins) components, with the sizes of the arrows or dots dictate their magnitudes.

basis for the quantum case, a many-body classical field can be expressed as a direct sum of local vector spaces. We construct the local vector space from the irreps of a symmetry group defined on a local network of spins within a plaquette p, invariant under a lattice point group G:

$$\mathcal{S}_p = \bigoplus_{i\in p} S_i. \tag{1}$$

$S_i = (S_i^x \ S_i^y \ S_i^z)^T \in \mathsf{O}_i(3)$ at the i^{th} site, and $\mathcal{S}_p \in \mathsf{O}_p(3n)$ where n is the number of sublattices in p. ($\mathsf{O}_i(n)$, $\mathsf{O}_p(n)$ distinguish the orthogonal symmetry of the site and plaquette fields, respectively). We denote the irreps of G by $m_\alpha \in \mathbb{R}$, and its vector representation by $\mathcal{M} = \bigoplus_\alpha d_\alpha m_\alpha$, where α runs over distinct irreps, and $d_\alpha \in \mathbb{Z}$ denotes their multiplets. The transformation from the spin space to the irreps space involves an orthogonal matrix, whose column vectors $\mathcal{V}_\alpha$ form the orthonormal basis of the irreps representation. Expressing $\mathcal{S}_p$ in this irreps space yields

$$\mathcal{S}_p = \sum_{\alpha=1}^{3n} m_\alpha \mathcal{V}_\alpha. \tag{2}$$

(The plaquette index is implicit in m, $\mathcal{V}$.) Interestingly, m_α conforms to Landau's order parameter as the coarse-grain average of local fields, except, here it is invariant under discrete symmetry group in a plaquette and is interpreted as the probability amplitude of vector field: $m_\alpha = \mathcal{V}_\alpha^T \mathcal{S}_p$. The local spins are the fragmented entities in the irreps space, defined by a rectangular projection matrix $\mathcal{P}_{i\in p}$ as $\mathbf{S}_{i\in p} = \mathcal{P}_{i\in p}\mathcal{S}_p = \sum_\alpha m_\alpha \mathcal{P}_{i\in p}\mathcal{V}_\alpha$.

Reformulating the order parameters in terms of the irreps conveniently decouples them in a symmetry invariant Hamiltonian, albeit the irreps' multiples can mix among themselves. To account for the multiplets' submanifold and emergent symmetry, it is convenient to introduce an $\mathsf{O}_p(d_\alpha)$ 'spinor'-like field $\boldsymbol{m}_\alpha := (m_\alpha^{(1)} \ ... \ m_\alpha^{(d_\alpha)})^T$ for the α irrep. Then, the eigenmodes are obtained by orthogonal rotation $\tilde{\boldsymbol{m}}_\alpha = e^{i\boldsymbol{\mathcal{L}}_\alpha\cdot\boldsymbol{\phi}_\alpha}\boldsymbol{m}_\alpha$, where $\boldsymbol{\mathcal{L}}_\alpha$ are the corresponding generators for the angle $\boldsymbol{\phi}_\alpha$. $\boldsymbol{\phi}_\alpha$ lives on the Hamiltonian's parameter space and assumes fixed values for the energy eigenmodes. The orthonormal basis states ensure the constraint $|\mathcal{S}_p|^2 = \sum_\alpha d_\alpha |m_\alpha|^2 = nS^2$, $\forall p$, where $|S_i| = S$, $\forall i$ is an additional hardcore constraint on the classical spins. Not all irreps necessarily adhere to the local constraint, requiring them to collaborate with others for existence. Such irreps ensembles may lead to non-analyticity and fragmentation into an order-disorder mixed phase. Additionally, the collapse of the eigenmodes $\tilde{\boldsymbol{m}}_\alpha$ into its constituent irrep $\boldsymbol{m}_\alpha$ causes distinct fragmented excitation.

We have a $3nN$-dimensional vector space $\mathcal{S} = \bigoplus_p \mathcal{S}_p$ for a generic N-unit cell lattice, commencing a $3nN \times 3nN$-matrix valued quadratic-in-spin Hamiltonian. However, thanks to nearest-neighbor interaction and discrete-translation-invariance of the lattice, the Hamiltonian can be brought to a block-diagonal form in terms of the plaquette Hamiltonian H_p:

$$H_p = \frac{1}{2}\mathcal{S}_p^T \mathcal{H}_p \mathcal{S}_p. \tag{3}$$

Here $\mathcal{H}_p$ is an orthogonal matrix-valued Hamiltonian, analogous to the second quantized Hamiltonian, whose components consist of all possible interactions between $\mathbf{S}_i$ and $\mathbf{S}_j$ for $\langle ij\rangle \in p$. However, lattice symmetries restrict the allowed finite components in $\mathcal{H}_p$, which we now consider for a square kagome lattice.

Realizations in a square-Kagome lattice: The square-Kagome lattice belongs to the Dihedral D_4 group with $n = 8$ sublattice spins, giving a 24-dimensional vector representation. Denoting the group element $\mathsf{g} \in \mathsf{D}_4$ in the $\mathcal{S}_p-$representation by the matrix-valued operators $\mathcal{D}(\mathsf{g})$, we impose the symmetry criterion that under a local symmetry transformation $\mathcal{S}_p \to \mathcal{D}(\mathsf{g})\mathcal{S}_p$, the local Hamiltonian H_p is invariant if $[\mathcal{D}(\mathsf{g}), \mathcal{H}_p] = 0$, $\forall p, \mathsf{g}$. Since local $\mathsf{O}_i(3)$ and sublattice symmetries are abandoned, the plaquette symmetry allows us to have bond- and spin-dependent interactions $J_{ij}^{\mu\nu}$ with six exchange and three DM interactions (see *SM* for the details), leading to a bond-dependent XYZ-Heisenberg model with XY-DM interaction. However, imposing bond-independent interactions, we consider an XXZ model with DM interaction as more appropriate for realistic materials [41–43], $H = \sum_{\langle ij\rangle,\mu\nu} J^{\mu\nu} S_i^\mu S_j^\nu$. This can, for future convenience, be expressed as:

$$H = J \sum_{\langle ij\rangle,\tau=\pm} \left(D^\tau e^{\mathrm{i}\tau(\Theta_i+\Theta_j)} S_i^\perp S_j^\perp + \Delta S_i^z S_j^z \right). \tag{4}$$

Here $J^{\mu\nu} = J\delta_{\mu\nu} + JD\epsilon_{\mu\nu}$ for $\mu = x, y$, and $J^{zz} = J\Delta$, $\delta_{\mu\nu}$ is the Kronecker delta and $\epsilon_{\mu\nu}$ is the Levi-Civita tensor. J is the exchange term, Δ is the z-axis anisotropy

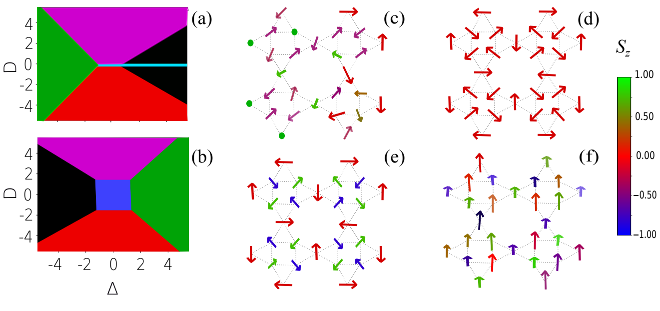

FIG. 2. Computed phase diagrams within the Monte Carlo simulation are shown for (a) for AFM ($J = +1$) and (b) for the FM ($J = -1$) couplings. We highlight spin textures in a randomly chosen four-plaquette setting for representative phases. The displayed phases are (c) AFM CSL at $(J, \Delta, D) = (1, 1, 0)$, (d) Anti-vortex order at $(1, 0, -3)$, (e) Fragmented phase at $(1, 4, -1)$ where S_i^z values are random while $S_i^{\perp}$ are ordered in a staggered AFM-anti-vortex texture, (f) Fragmented phase at $(-1, -2.5, 0)$ where S_i^z is disorder while $S_i^{\perp}$ exhibit collinear ordering.

ratio, and JD is the XY DM interaction strength. By diagonalizing the tensor $J^{\mu\nu}$, we define two 'circularly polarized' fields: $S_i^{\tau} = |S_i^{\perp}|e^{\mathrm{i}\tau\Theta_i} \in \mathsf{O}_i(2) \cong \mathsf{U}_i(1)$, where $S_i^{\perp} = \sqrt{S^2 - (S_i^z)^2}$ is the coplanar spin magnitude and Θ_i is the azimuthal angle in the spin space, which interact via a complex (dimensionless) interaction $D^{\tau} = 1 + \mathrm{i}\tau D$.

Irreps in square-Kagome lattice: There are five conjugacy classes in this non-Abelian group, giving five irreps: $m_\alpha \equiv \mathsf{A}_{1,2}^{(d_\alpha)}$, $\mathsf{B}_{1,2}^{(d_\alpha)}$, and a two-dimensional $\mathsf{E}^{(d_\alpha)}$, where the superscript denotes their multiplicity $(d_\alpha) = (2, 4, 3, 3, 6)$, respectively. Representative irreps configurations are shown in Fig. 1(b).

We organize these irreps into an out-of-plane set $\mathsf{m}_z := \{\mathsf{A}_2^{(\mathrm{c,d})}, \mathsf{B}_{1,2}^{(\mathrm{c})}, \mathsf{E}^{(\mathrm{e,f})}\}$, and a coplanar set:$\mathsf{m}_\perp := \mathsf{m}_z^{\complement}$. Coplanar irreps $\mathsf{A}_{1,2}^{(\mathrm{a,b})}$, $\mathsf{B}_{1,2}^{(\mathrm{a,b})}$ are even and odd under C_4, forcing S_i^{τ} to obey a homeomorphism $\Theta_{i\in p} = Q_p\theta_i + \gamma_p$, where Θ_i and θ_i are the (local) azimuthal angles in the spin and position manifolds, respectively, $\gamma_p \in [0, \pi)$ is the (global in p) helicity angle, and $Q_p \in \pi_1(\mathbb{S}^1) \cong \mathbb{Z}$ is the topological charge. As shown in Fig. 1(b), this leads to two concentric (anti-/) vortex substructures in the outer and inner squares within each plaquette, which are unrelated by symmetry and interact solely through D^{τ}. $\mathsf{A}_1^{(\mathrm{a,b})}$ consist of concentric vortices with the same/opposite helicities ($\gamma_p = \pm\pi/2$), while $\mathsf{A}_2^{(\mathrm{a,b})}$, odd under reflection, have $\gamma_p = \pm\pi$. $\mathsf{B}_{1,2}^{(\mathrm{a,b})}$ irreps (odd under $\mathcal{C}_4$) are similar, except they consist of anti-vortices. The out-of-plane $\mathsf{A}_2^{(\mathrm{c,d})}$ are colinear FM/AFM irreps, while $\mathsf{B}_{1,2}^{(\mathrm{c})}$ are colinear AFM irreps that do *not* satisfy the local constraint. Finally, among the six-fold multiplets of E irrep, $\mathsf{E}^{(\mathrm{a-d})}$ are co-planer FM/ nematic/AFMorder parameters, while $\mathsf{E}^{(\mathrm{e,f})}$ are out-of-plane irreps that violate the local constraints.

Eigen energies: The final task is to diagonalize the multiples of the irreps. In our case, the irreps' multiplets split as either $\mathsf{O}_p(d_\alpha) = \mathsf{O}_p(2) \oplus \mathsf{O}_p(2) \oplus ...$, or $\mathsf{O}_p(d_\alpha) = \mathsf{O}_p(2) \oplus \mathsf{Z}_2 \oplus ...$, in which all $\mathsf{O}_p(2)$ operators have the same generator $\mathcal{L}_\alpha = i\sigma_y$. ϕ_α depends only on $\arg(\mathrm{D}^{\tau})$ in the eigenstates of $\mathcal{H}_p$. The resultant diagonal Hamiltonian per plaquette is

$$H_p = \sum_{\nu=1}^{3n} E_\nu |\tilde{\mathbf{m}}_\nu|^2. \tag{5}$$

Here $|\tilde{\mathbf{m}}_\nu|^2$ serves as an 'occupation density' to the ν^{th} order parameter's energy level E_ν. We, henceforth, omit the tilde symbol for simplicity, and all irreps are taken to be eigenmodes unless mentioned otherwise. Constrained by symmetry, $E_{\nu\in\mathsf{m}_\perp}$ depends solely on D^{τ}, while $E_{\nu\in\mathsf{m}_z}$ are proportional to Δ [49]. One or more irrep (s) can form a uniform (order) phase with a global energy minimum at NE_ν if they satisfy the constraint and frustration; otherwise, they blends with other irreps to form a degenerate ensemble, distributing randomly in the lattice.

Phase diagrams and correlation functions: Using classical Monte-Carlo simulations of Eq.$\tilde{(}4)$ under the imposed local constraint, we generate the phase diagram presented in Fig. 2. Notably, across all phases (ordered, disordered, and fragmented), the spin texture within each plaquette adheres to the irreps, which permits us to construct a many-body ground state vector field for all phases:

$$\mathcal{S}_{\mathrm{GS}} = \bigoplus_p \sum_{\{\nu_p\}} m_{\nu_p} \mathcal{V}_{\nu_p}. \tag{6}$$

The ordered phase harbors a summated state of a fixed irrep $\bar{\nu} \in \{\nu_p\}$ (with $m_{\bar{\nu}} = \bar{m}$, $m_{\nu\neq\bar{\nu}} = 0$, $\forall p$); while the staggered phase features two alternating but fixed irreps $\bar{\nu}_p$ and $\bar{\nu}_q$ in neighboring plaquettes. The CSL state, on the other hand, combines a dynamic ensemble of irreps $\{\nu_p\}$ within each plaquette p. Within this ensemble, the probability amplitude m_{ν_p} may vary randomly, subject to local constraints, for the same plaquette energy. The random distribution of m_{ν_p} differs between plaquettes, resulting in an extensively degenerate ground state.

In addition to the consistency between the unbiased Monte-Carlo simulation and the irreps constructions, we also compare our results with a soft-spin approximation in the Fourier space ([4, 6, 34, 50–52] and see *SM*). Given that we have experimental access to the correlation function of local spins $\mathbf{S}_{i\in p}$, we report its correlation function. We project the structure factor $\chi(\mathbf{k}) = 1/\mathcal{N}\sum_{i,j}\langle \mathbf{S}_i \cdot \mathbf{S}_j\rangle \exp\left(\mathrm{i}\mathbf{k}\cdot(\mathbf{r}_i - \mathbf{r}_j)\right)$ to the irreps space as

$$\langle \mathbf{S}_i \cdot \mathbf{S}_j \rangle = \sum_{\nu_p\nu_q} m_{\nu_p} m_{\nu_q} \langle \mathcal{V}_{\nu_p}^T \mathcal{P}_i^T \mathcal{P}_j \mathcal{V}_{\nu_q}\rangle, \tag{7}$$

with $\mathbf{r}_i$ is the i^{th} spin's position in p and $j \in q$ plaquette.

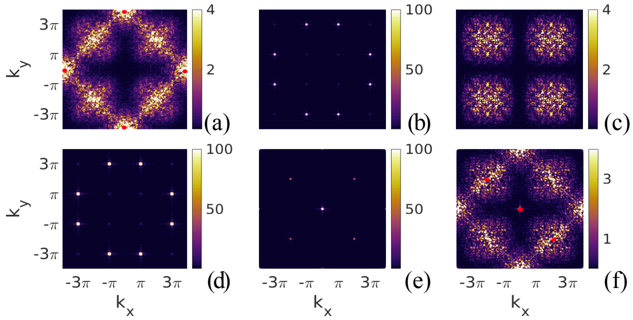

FIG. 3. Simulated static structure factors are plotted in the momentum space for the four phases discussed in Fig. 2. (a) AFM CSL at $(J, \Delta, D) = (1, 1, 0)$, where red dots are plotted separately to signify additional strong Bragg-like peaks that overwhelm the spectral density of the disordered pattern. (b-c) Fragmented phase at $(1, 4, -1)$ where the plots for the ordered $S_i^{\perp}$ and disordered S_i^z components are separated in (b) and (c), respectively. (d) Anti-vortex order at $(1, 0, -3)$ showing Bragg peaks similar to $S_i^{\perp}$ components in (b). (e-f) Fragmented phase at $(-1, -2.5, 0)$ with FM ordered $S_i^{\perp}$ and disorder S_i^z are separated in (e) and (f). Panels (a) and (f) host pinch-points around $(\pi, 3\pi)$ and its equivalent points.

The phase diagram reveals a predominance of (uniform or staggered) order phases in both $J < 0$ (frustration inactive) and $J > 0$ (frustration active) regions, with a CSL phase emerging at the critical line of $D \to 0$, otherwise, it turns into distinct mixed phases for $2|D|/\Delta < 1$. For $D \to 0$, $J > 0$, three distinct CSL phases emerge with varying Δ. At $D = 0$, the coplanar irreps $\mathsf{A}_{1,2}^{(\mathrm{a,b})}$, $\mathsf{B}_{1,2}^{(\mathrm{a,b})}$ become degenerate at $-2J$, while $\mathsf{E}^{(\mathrm{c,d})}$, satisfying the constraint but not frustration, have the lowest energy at $-4J$. As $\Delta \to 0$, the Hamiltonian (first term in Eq. 4) is constrained by a local $\mathsf{O}_i(2)$ symmetry of the S_i^{τ} fields, and the structure factor $\chi(\mathbf{k})$ receives only finite contribution from S_i^{τ} and no allocation to S_i^z. Moreover, $\chi(\mathbf{k})$ displays a characteristic disorder pattern without any Bragg-like peak but with a prominent pinch-point around $\mathbf{k} = (\pm\pi, \pm 3\pi)$. The pinch-point characterizes an algebraic correlation between the topological charge of the $\mathsf{O}_p(2)$ multiplets. At $\Delta = 1$, the Hamiltonian is subject to a full $\mathsf{O}_i(3)$ symmetry constraint per site, resulting in symmetry-allowed access to the entire ensemble $\{m_{\nu_p}\} \subseteq \mathsf{m}_{\perp} \cup \mathsf{m}_z$. For example, $\{m_{\nu}\} \in \{\mathsf{A}_{1,2}^{(\mathrm{a,b,c,d})}, \mathsf{B}_{1,2}^{(\mathrm{a,b})}\}$ are degenerate at $E_{\nu} = -2J$ and $\{m_{\nu'}\} \in \{\mathsf{B}_{1,2}^{(\mathrm{c})}, \mathsf{E}^{(\mathrm{c,d})}\}$ at $E_{\nu'} = -4J$, making a larger CSL ensemble degenerate at energy $E_p = m_{\nu}^2 E_{\nu} + m_{\nu'}^2 E_{\nu'} = -4J$ for $m_{\nu} = \sqrt{2} m_{\nu'}$. Consequently, $\chi(\mathbf{k})$ displays pinch-point correlations among both S_i^{τ} and S_i^z. Finally, as $\Delta \to \infty$, the Hamiltonian (last term in Eq. 4) retains a residual local Z_2 symmetry constraint, and the disorder ground state solely stems from the $\{m_{\nu_p}\} \subseteq \mathsf{m}_z$ ensemble. $\chi(\mathbf{k})$ is contributed solely by S_i^z with pinch-points at $\mathbf{k} = (\pm\pi, \pm\mathbf{3}\pi)$. Based on their distinct local constraints, it is convenient to refer to these phases as $\mathsf{O}(2)$, $\mathsf{O}(3)$, and Z_2 CSLs, respectively, without implying a Landau-type phase boundary between them.

Any finite D steers the CSL phase into either order or fragmented (mixed) phases. For weak out-of-plane anisotropy $\Delta < 2|D|$, D^{τ} ($\tau = \mathrm{sgn}(D)$) interaction uniformly selects a coplanar irrep $m_{\mathsf{B}_1/\mathsf{A}_1}$ containing concentric (anti-/) vortices, respectively (red/magenta regions in Fig. 2). Here, the (anti-/) vortices of the same topological charge are staggered between the neighboring plaquettes with a $\gamma_p = \pi$ phase shift, with Bragg-like peaks at $\mathbf{k} = (\pi, \pi)$ in $\chi(\mathbf{k})$. However, for strong $\Delta > 2|D|$ (and $J > 0$), the homogenous coplanar order becomes scrambled with disordered out-of-plane irreps: $\{m_{\nu_p}\}_{\mathrm{mix}} \subseteq m_{\mathsf{A}_1/\mathsf{B}_1} \cup \mathsf{m}_z$, in Fig. 2(e). Their interplay yields an interesting fragmentation feature in which the outer vortex maintains coplanarity, while the inner vortex mixes with the $\mathsf{B}_1^{(\mathrm{c})} \in \mathsf{m}_z$ irrep in each plaquette. The combination $m_{\mathsf{A}_1} = -m_{\mathsf{B}_1}$ produces a novel *AFM-vortex/AFM-anti-vortex* texture within the inner square where neighboring spins possess opposite easy axes [53]. Consequently, $\mathsf{O}_i(3)$ field fragments into its S_i^z components becoming non-interacting and fail to order or exhibit any significant correlation, while the S_i^{τ} fields exhibit long-range order with Bragg-like peaks in the structure factor, see Fig. 3(b). In essence, this is a unique spin liquid-crystal-like phase arising from a coordinated spatial distribution of the probability amplitude (m_{α}) of the contributing irreps.

The interplay between the FM interaction, $J = -1$, and strong AFM out-of-plane anisotropy $\Delta > 2|D|$ generates fragmented phases of distinct characteristics. Here, the in-plane FM irrep $\mathsf{E}^{(\mathrm{a,b})}$ pairs with the out-of-plane AFM $\mathsf{E}^{(\mathrm{f})}$ counterpart. The latter violates the local constraint, leading to an intriguing fragmented structure in $\chi(\mathbf{k})$, showing a FM ordering in S_i^{τ}, but a pinch-point disorder in S_i^z. This irreps ensemble satisfies $m_{\mathsf{E}^{(\mathrm{a})}} = m_{\mathsf{E}^{(\mathrm{b})}} = m_{\mathsf{E}^{(\mathrm{f})}}/\sqrt{2}$, but an extensive degeneracy arises from the possibilities of the four-fold orientations of the $\mathsf{E}^{(\mathrm{f})}$ irrep, see Fig. 1(b). The DM interaction disfavors this mixed phase for $D > 2\Delta$, leading to a transition to similar in-plane orders of (anti-/) vortices observed in the $J = 1$ phase diagram. The remaining two phases are readily identifiable: a uniform coplanar FM order with $\bar{m}_{\mathsf{E}^{(\mathrm{a_y})}}$ irrep at $\Delta \to 0$, and an out-of-plane FM order with $\bar{m}_{\mathsf{A}_2^{(\mathrm{c})}}$) for $J\Delta \to \infty$.

Conclusions and outlook. We followed an analysis that draws parallels between quantum and classical field theories in the context of spin liquids and fractionalization. While the distinction lies in the quantum statistics manifesting as a direct product basis versus a direct summated field, the concept of superposition and symmetry group representation remain central to both. This shared concept underpins the emergence of fragmentation and spin liquid ground states. Discussions on their excitations and phase transition are merited. Among the ordered phases, the (anti-/) vortex order phases (red and magenta) exhibit novel collective excitations. As their descriptions are equivalent, we discuss the vortex case here. Gapless collective excitations emerge from the long-wavelength fluctuation of the helicity angle γ_p across the lattice, protected by the topology of the irreps space through the charge $Q_p \in \mathbb{Z}$. These modes, termed helicity phase modes or phasons, possess novel characteristics. The two concentric vortices per plaquette are coupled by interaction but not symmetry. Frustration affects only the outer vortex, resulting in the fragmentation of the excitation spectrum into a collective mode for the ordered fields and local excitations for the disordered components. The Mermin-Wagner theorem dictates the instability of ordered states to gapless magnons or phason modes, while disorder phases tend to order via thermal fluctuations according to the order-by-disorder paradigm [14, 16–18]. Notably, the two ordered phases of vortex and anti-vortices for $\pm D$ consists of different irreps, i.e., distinct conjugacy classes that do not couple in the Hamiltonian. Hence their phase boundary at $D = 0$ signifies a topological phase transition, associated with a spin liquid phase at the critical point, reminiscence of the deconfined critical point [54]. The CSL critical point can be extended by applying a magnetic field in the z-direction (see *SM*). Moreover, transitions between ordered and fragmented phases, or within fragmented phases, offer intriguing avenues for studying non-Landau-type phase transitions.

Acknowledgements: TD acknowledges research funding from the S.E.R.B. Department of Science and Technology, India, under Core Research Grant (CRG) Grant No. CRG/2022/00341 and acknowledges the computational facility at S.E.R.C. Param Pravega under NSM grant No. DST/NSM/R&D HPC Applications/2021/39.

[1] L. Balents, Nature **464**, 199 (2010).
[2] C. L. Henley, Annual Review of Condensed Matter Physics **1**, 179 (2010).
[3] R. Moessner and J. T. Chalker, Phys. Rev. Lett. **80**, 2929 (1998).
[4] J. Rehn, A. Sen, K. Damle, and R. Moessner, Phys. Rev. Lett. **117**, 167201 (2016).
[5] O. Benton, L. Jaubert, H. Yan, and N. Shannon, Nature Communications **7**, 10.1038/ncomms11572 (2016).
[6] O. Benton and R. Moessner, Phys. Rev. Lett. **127**, 107202 (2021).
[7] C. Castelnovo, R. Moessner, and S. Sondhi, Annual Review of Condensed Matter Physics **3**, 35–55 (2012).
[8] C. Nisoli, R. Moessner, and P. Schiffer, Rev. Mod. Phys. **85**, 1473 (2013).
[9] K. A. Ross, L. Savary, B. D. Gaulin, and L. Balents, Phys. Rev. X **1**, 021002 (2011).
[10] M. E. Brooks-Bartlett, S. T. Banks, L. D. C. Jaubert, A. Harman-Clarke, and P. C. W. Holdsworth, Phys. Rev. X **4**, 011007 (2014).
[11] S. Powell, Phys. Rev. B **91**, 094431 (2015).
[12] S. Petit, E. Lhotel, B. Canals, M. Ciomaga-Hatnean, J. Ollivier, H. Mutka, E. Ressouche, A. R. Wildes, M. R. Lees, and G. Balakrishnan, Observation of magnetic fragmentation in spin ice (2016), arXiv:1603.05008 [cond-mat.str-el].
[13] B. Canals, I.-A. Chioar, V.-D. Nguyen, M. Hehn, D. Lacour, F. Montaigne, A. Locatelli, T. O. Menteş, B. S. Burgos, and N. Rougemaille, Nature Comm. **7**, 10.1038/ncomms11446 (2016).
[14] Villain, J., Bidaux, R., Carton, J.-P., and Conte, R., J. Phys. France **41**, 1263 (1980).
[15] C. L. Henley, Phys. Rev. Lett. **62**, 2056 (1989).
[16] P. Chandra, P. Coleman, and A. I. Larkin, Phys. Rev. Lett. **64**, 88 (1990).
[17] J. T. Chalker, P. C. W. Holdsworth, and E. F. Shender, Phys. Rev. Lett. **68**, 855 (1992).
[18] E. F. Shender and P. C. W. Holdsworth, Order by disorder and topology in frustrated magnetic systems, in *Fluctuations and Order: The New Synthesis*, edited by M. Millonas (Springer US, New York, NY, 1996) pp. 259–279.
[19] A. Pizzi, A. Nunnenkamp, and J. Knolle, Phys. Rev. Lett. **127**, 140602 (2021).
[20] B. Placke, O. Benton, and R. Moessner, Ising fracton spin liquid on the honeycomb lattice (2023), arXiv:2306.13151 [cond-mat.str-el].
[21] D. Dahlbom, H. Zhang, Z. Laraib, D. M. Pajerowski, K. Barros, and C. Batista, Renormalized classical theory of quantum magnets (2023), arXiv:2304.03874 [cond-mat.str-el].
[22] R. P. Nutakki, L. D. C. Jaubert, and L. Pollet, SciPost Phys. **15**, 040 (2023).
[23] N. Davier, F. A. Gómez Albarracín, H. D. Rosales, and P. Pujol, Phys. Rev. B **108**, 054408 (2023).
[24] H. Yan, O. Benton, R. Moessner, and A. H. Nevidomskyy, Classification of classical spin liquids: Typology and resulting landscape (2023), arXiv:2305.00155 [cond-mat.str-el].
[25] H. Yan, O. Benton, A. H. Nevidomskyy, and R. Moessner, Classification of classical spin liquids: Detailed formalism and suite of examples (2023), arXiv:2305.19189 [cond-mat.str-el].
[26] Y. Fang, J. Cano, A. H. Nevidomskyy, and H. Yan, Classification of classical spin liquids: Topological quantum chemistry and crystalline symmetry (2023), arXiv:2309.12652 [cond-mat.str-el].
[27] K. Essafi, O. Benton, and L. Jaubert, Nature Communications **7**, 10.1038/ncomms10297 (2016).
[28] H. Yan, O. Benton, L. Jaubert, and N. Shannon, Phys. Rev. B **95**, 094422 (2017).
[29] K. Essafi, O. Benton, and L. D. C. Jaubert, Phys. Rev. B **96**, 205126 (2017).
[30] S. T. Bramwell, Philosophical Transactions of the Royal Society A: Mathematical, Physical and Engineering Sciences **370**, 5738 (2012).
[31] L. Savary and L. Balents, Phys. Rev. Lett. **108**, 037202 (2012).
[32] R. Siddharthan, B. S. Shastry, A. P. Ramirez, A. Hayashi, R. J. Cava, and S. Rosenkranz, Phys. Rev. Lett. **83**, 1854 (1999).

[33] S. T. Bramwell and M. J. P. Gingras, Science **294**, 1495 (2001).

[34] S. V. Isakov, K. Gregor, R. Moessner, and S. L. Sondhi, Phys. Rev. Lett. **93**, 167204 (2004).

[35] L. A. S. Mól, A. R. Pereira, and W. A. Moura-Melo, Phys. Rev. B **85**, 184410 (2012).

[36] Y. Li, P. Gegenwart, and A. A. Tsirlin, Journal of Physics: Condensed Matter **32**, 224004 (2020).

[37] D. T. Liu, F. J. Burnell, L. D. C. Jaubert, and J. T. Chalker, Phys. Rev. B **94**, 224413 (2016).

[38] Y. Iqbal, H. O. Jeschke, J. Reuther, R. Valentí, I. I. Mazin, M. Greiter, and R. Thomale, Phys. Rev. B **92**, 220404 (2015).

[39] T. Mizoguchi, L. D. C. Jaubert, and M. Udagawa, Phys. Rev. Lett. **119**, 077207 (2017).

[40] T. Yildirim, A. B. Harris, and E. F. Shender, Phys. Rev. B **58**, 3144 (1998).

[41] M. Fujihala, K. Morita, R. Mole, S. Mitsuda, T. Tohyama, S.-i. Yano, D. Yu, S. Sota, T. Kuwai, A. Koda, *et al.*, Nat. Commun. **11**, 3429 (2020).

[42] O. V. Yakubovich, L. V. Shvanskaya, G. V. Kiriukhina, A. S. Volkov, O. V. Dimitrova, and A. N. Vasiliev, Inorganic Chemistry **60**, 11450 (2021), pMID: 34264636.

[43] M. M. Markina, P. S. Berdonosov, T. M. Vasilchikova, K. V. Zakharov, A. F. Murtazoev, V. A. Dolgikh, A. V. Moskin, V. N. Glazkov, A. I. Smirnov, and A. N. Vasiliev, Static and resonant properties of decorated square kagome lattice compound $KCu_7(TeO_4)(SO_4)_5\,Cl$ (2023), arXiv:2212.11623 [cond-mat.str-el].

[44] N. Astrakhantsev, F. Ferrari, N. Niggemann, T. Müller, A. Chauhan, A. Kshetrimayum, P. Ghosh, N. Regnault, R. Thomale, J. Reuther, T. Neupert, and Y. Iqbal, Phys. Rev. B **104**, L220408 (2021).

[45] J. Richter, O. Derzhko, and J. Schnack, Phys. Rev. B **105**, 144427 (2022).

[46] N. Niggemann, N. Astrakhantsev, A. Ralko, F. Ferrari, A. Maity, T. Müller, J. Richter, R. Thomale, T. Neupert, J. Reuther, Y. Iqbal, and H. O. Jeschke, Phys. Rev. B **108**, L241117 (2023).

[47] J. Richter and J. Schnack, Phys. Rev. B **107**, 245115 (2023).

[48] M. Gembé, H.-J. Schmidt, C. Hickey, J. Richter, Y. Iqbal, and S. Trebst, Phys. Rev. Res. **5**, 043204 (2023).

[49] Specifically, the (anti-/) vortex irreps $\mathsf{B}_{1,2}^{(\mathrm{a,b})}$, $\mathsf{A}_{1,2}^{(\mathrm{a,b})}$ are promoted by $\mp D$, while $\mathsf{E}^{(\mathrm{a,b})}$ do not depend on D.

[50] P. H. Conlon and J. T. Chalker, Phys. Rev. Lett. **102**, 237206 (2009).

[51] P. H. Conlon and J. T. Chalker, Phys. Rev. B **81**, 224413 (2010).

[52] J. Rehn, A. Sen, and R. Moessner, Phys. Rev. Lett. **118**, 047201 (2017).

[53] This AFM-vortex topology is homotopically distinct from the known AFM skyrmion[**?**], and has not been predicted previously.

[54] T. Senthil, A. Vishwanath, L. Balents, S. Sachdev, and M. P. A. Fisher, Science **303**, 1490 (2004).

SUPPLEMENTARY MATERIAL

DETAILED DERIVATION OF THE SYMMETRY PROPERTIES

Here, we provide further details of the relevant mathematical constructions that are used in the main text. We start with a system of $\mathcal{N}$ spins. Much like how one starts in the quantum case with a direct product state basis to construct exotic entangled states, here we can also start with a many-body $3\mathcal{N}$-dimensional vector field as a direct sum basis: $\mathcal{S} = \oplus_i^{\mathcal{N}} \mathbf{S}_i$, where $\mathbf{S}_{i=1} \in \mathsf{O}(3)$. Then, the most general two-spin interaction Hamiltonian is written as $H = \mathcal{S}^T \mathcal{H} \mathcal{S}$, where $\mathcal{H}$ is the $3\mathcal{N} \times 3\mathcal{N}$ matrix-valued Hamiltonian. Short-range interaction and (discrete) translational symmetry drastically simplifies this Hamiltonian, giving a block-diagonal one.

We assume that there exists a unit cell with sublattices that are invariant under a point group symmetry G. The spins sitting at the cell coordinates interact with the spins from the neighboring cells. This interaction term is translated back to a periodically equivalent interaction between the spins within the cell. This allows us to define a plaquette containing n sublattices (counting the sites fully that are shared with the neighboring cells, and hence, the number of sublattices in a plaquette is larger than that in a periodic cell). In this prescription, the Hamiltonian $\mathcal{H}$ becomes block diagonal into a $3n \times 3n$ plaquette Hamiltonian $\mathcal{H}_p$, and the many-body spin vector field splits as $\mathcal{S} = \oplus_{p=1}^{N=\mathcal{N}/n} \mathcal{S}_p$, where $\mathcal{S}_p$ the vector field in the plaquette.

Here, we focus on the square Kagome lattice, which has $n = 8$ sites in a plaquette, giving a 24-dimensional reducible representation $\mathcal{S}_p$, as shown in Fig. X. Our first job is to find the irreducible representation of the Dihedral group D_4 group in this vector field representation. The group elements are denoted by $\mathsf{D}_4 = \{e, \mathsf{C}_4, \mathsf{C}_4^2, \mathsf{C}_4^3, \sigma_v^x, \sigma_v^y = \mathsf{C}_4^{-1}\sigma_v^x\mathsf{C}_4, \sigma_v^{xy}, \sigma_v^{yx} = \mathsf{C}_4^{-1}\sigma_v^{xy}\mathsf{C}_4\}$, where C_4 is the four-fold rotation, σ_v are the reflection with respect to the verticle plane passing through the $x, y-$ axis, or diagonal (xy/yx), as shown in Fig. X. In this $\mathcal{S}_p$-representation, we can split each of the D_4 group elements as successive transformations on how the onsite spin $\mathbf{S}_i \in \mathsf{O}(3)$ undergoes an internal spin rotation, followed by how each component $S^{\mu}_{i=1-8}$ of the 8 sublattices reorders in the plaquette vector $\mathcal{S}_p$. Noticeably further, the inner and outer squares of the square kagome lattice are decoupled from each other in terms of the D_4 symmetries and give a trivial transformation between the two concentric squares of four sublattices. In what follows, if we denote the $\mathcal{S}_p$-representation of the group elements $\mathsf{g} \in \mathsf{D}_4$ as $\mathcal{D}(\mathsf{g})$, then it can be decomposed into a direct product of three symmetries: $\mathcal{D}(\mathsf{g}) = \mathcal{R}_I(\mathsf{g}) \otimes \mathcal{R}_L(\mathsf{g}) \otimes \mathcal{R}_S(\mathsf{g})$, where $\mathcal{R}_S(\mathsf{g})$ are the 3×3 rotational matrices of the local $\mathsf{O}_i(3)$ spin, $\mathcal{R}_L(\mathsf{g})$ are the 4×4 rotational matrices of the four sublattices, and $\mathcal{R}_I(\mathsf{g})$ is the 2×2 transformation between the inner and outer squares.

$$
\begin{aligned}
\mathcal{D}(\mathsf{C}_4) &= \left[\tau_0 \otimes \mathcal{R}_L^{(1)}(\mathsf{C}_4) + \tau_x \otimes \mathcal{R}_L^{(2)}(\mathsf{C}_4)\right] \otimes \mathcal{R}_S(\mathsf{C}_4),\\
\mathcal{D}(\mathsf{C}_4^2) &= \tau_x \otimes \mathbb{I}_{4\times 4} \otimes \mathcal{R}_S(\mathsf{C}_4^2),\\
\mathcal{D}(\mathsf{C}_4^3) &= \left[\tau_0 \otimes \mathcal{R}_L^{(2)}(\mathsf{C}_4) + \tau_x \otimes \mathcal{R}_L^{(1)}(\mathsf{C}_4)\right] \otimes \mathcal{R}_S(\mathsf{C}_4^3),\\
\mathcal{D}(\sigma_v^x) &= \left[\tau_0 \otimes \mathcal{R}_L^{(1)}(\sigma_v^x) + \tau_x \otimes \mathcal{R}_L^{(2)}(\sigma_v^x)\right] \otimes \mathcal{R}_S(\sigma_v^x),\\
\mathcal{D}(\sigma_v^y) &= \left[\tau_0 \otimes \mathcal{R}_L^{(2)}(\sigma_v^x) + \tau_x \otimes \mathcal{R}_L^{(1)}(\sigma_v^x)\right] \otimes \mathcal{R}_S(\sigma_v^y),\\
\mathcal{D}(\sigma_v^{xy}) &= \left[\tau_0 \otimes \mathcal{R}_L^{(1)}(\sigma_v^{xy}) + \tau_x \otimes \mathcal{R}_L^{(2)}(\sigma_v^{xy})\right] \otimes \mathcal{R}_S(\sigma_v^{xy}),\\
\mathcal{D}(\sigma_v^{yx}) &= \left[\tau_0 \otimes \mathcal{R}_L^{(2)}(\sigma_v^{xy}) + \tau_x \otimes \mathcal{R}_L^{(1)}(\sigma_v^{xy})\right] \otimes \mathcal{R}_S(\sigma_v^{yx}).
\end{aligned}
\tag{8}
$$

Here τ_0, τ_x are Pauli matrices defining the internal symmetry $\mathcal{D}_4(\mathsf{g})$, and

$$
\mathcal{R}_L^{(1)}(\mathsf{C}_4) = \begin{pmatrix} 0&0&0&0\\ 0&0&0&0\\ 1&0&0&0\\ 0&1&0&0 \end{pmatrix}, \mathcal{R}_L^{(2)}(\mathsf{C}_4) = \begin{pmatrix} 0&0&1&0\\ 0&0&0&1\\ 0&0&0&0\\ 0&0&0&0 \end{pmatrix}, \mathcal{R}_L^{(1)}(\sigma_v^x) = \begin{pmatrix} 0&0&0&0\\ 0&0&0&0\\ 0&0&0&0\\ 0&0&0&1 \end{pmatrix}, \mathcal{R}_L^{(2)}(\sigma_v^x) = \begin{pmatrix} 0&0&1&0\\ 0&1&0&0\\ 1&0&0&0\\ 0&0&0&0 \end{pmatrix},
$$
$$
\mathcal{R}_L^{(1)}(\sigma_v^{xy}) = \begin{pmatrix} 1&0&0&0\\ 0&0&0&0\\ 0&0&0&0\\ 0&0&0&0 \end{pmatrix}, \mathcal{R}_L^{(2)}(\sigma_v^{xy}) = \begin{pmatrix} 0&0&0&0\\ 0&0&0&1\\ 0&0&1&0\\ 0&1&0&0 \end{pmatrix}.
$$

Under C_4, the continuous $\mathsf{O}_i(3)$ symmetry simply becomes a discrete angle of rotation by $2\pi/4$ with L_z being the

D_4	d_α	E	$2C_4$	$2C_2''$	C_2	$2C_2'$
A_1	2	1	1	1	1	1
A_2	4	1	1	-1	1	-1
B_1	3	1	-1	1	1	-1
B_2	3	1	-1	-1	1	1
E	6	2	0	0	-2	0
S_p		24	0	-2	0	-2

TABLE S1. Character table of the group D_4. The last row corresponds to the characters of the reducible representation $\mathcal{S}_p$ for each class. $\mathrm{N}_k\mathrm{C}_k$ notion is used in the first row. N_k is the number of elements in each conjugacy class, C_k.

angular momentum, while under the mirror, spin is rotated as an axial vector. This gives

$$\mathcal{R}_S(\mathsf{C}_4) = \begin{pmatrix} 0 & -1 & 0 \\ 1 & 0 & 0 \\ 0 & 0 & 1 \end{pmatrix}, \quad \mathcal{R}_S(\sigma_v^x) = \begin{pmatrix} 1 & 0 & 0 \\ 0 & -1 & 0 \\ 0 & 0 & -1 \end{pmatrix}, \quad \mathcal{R}_S(\sigma_v^{xy}) = \begin{pmatrix} 0 & -1 & 0 \\ -1 & 0 & 0 \\ 0 & 0 & -1 \end{pmatrix}, \tag{9}$$

and $\mathcal{R}_S(\mathsf{C}_4^2) = (\mathcal{R}_S(\mathsf{C}_4))^2$, $\mathcal{R}_S(\mathsf{C}_4^3) = (\mathcal{R}_S(\mathsf{C}_4))^3$, $\mathcal{R}_S(\sigma_v^y) = \mathcal{R}_S(\mathsf{C}_4)^{-1}\mathcal{R}_S(\sigma_v^x)\mathcal{R}_S(\mathsf{C}_4)$, and $\mathcal{R}_S(\sigma_v^{yx}) = \mathcal{R}_S(\mathsf{C}_4)^{-1}\mathcal{R}_S(\sigma_v^{xy})\mathcal{R}_S(\mathsf{C}_4)$.

Symmetry of the Hamiltonian

The generic plaquette Hamiltonian is expressed in the main text as $H_p = \frac{1}{2}\mathcal{S}_p^T\mathcal{H}_p\mathcal{S}_p$, where $\mathcal{H}_p$ is the 24×24 *symmetric* matrix containing all possible nearest neighbor interactions. The symmetry constraints make many terms vanish or be identical to other terms. Under a symmetry, the vector field transforms to $\mathcal{S}_p' = \mathcal{D}(\mathsf{g})\mathcal{S}$, $\forall \mathsf{g} \in \mathsf{D}_4$, and if the Hamiltonian to H_p is invariant, then the Hamiltonian matrix transforms as $\mathcal{D}^T(\mathsf{g})\mathcal{H}_p\mathcal{D}(\mathsf{g}) = \mathcal{H}_p$, $\forall p$.

Under these conditions, we find that the interaction terms among the four triangles are related to each other by symmetry, while those within a triangle are independent of each other; see Fig. 1 (a). Consider the one independent triangle at sites $i = \{0, 1, 2\}$ in Fig. 1 (a), and we obtain three distinct 3×3 matrices between sites i and j :

$$(\mathcal{H}_p)_{01} = \begin{pmatrix} J^{xx} & D^{xy} & 0 \\ D^{yx} & J^{yy} & 0 \\ 0 & 0 & J^{zz} \end{pmatrix}, (\mathcal{H}_p)_{12} = \begin{pmatrix} J^{xx} & -D^{yx} & 0 \\ -D^{xy} & J^{yy} & 0 \\ 0 & 0 & J^{zz} \end{pmatrix}, \text{ and } (\mathcal{H}_p)_{20} = \begin{pmatrix} J'^{xx} & D'^{xy} & 0 \\ -D'^{xy} & J'^{yy} & 0 \\ 0 & 0 & J'^{zz} \end{pmatrix}. \tag{10}$$

Therefore, we have nine independent parameters: three exchange interactions $J^{\mu\mu}$, $J'^{\mu\mu}$. and three DM interactions D^{xy}, D^{yx}, and D'^{xy}. Due to in-plane inversion symmetry, no in-plane DM interaction is allowed. We take a simpler XXZ + DM interaction model in which $J^{\mu\mu} = J'^{\mu\mu}$, $J^{xx} = J^{yy} = J^{zz}/\Delta = J$, and $D^{xy} = -D^{yx} = D'^{xy} = JD$. This gives us three independent parameters, among which the global energy scaling by J is removed, except its sign $\pm$ is considered in the main text.

Irreducible spin configurations

Finally, we find the irreducible representation of the $\mathcal{S}_p$ vector. There are five classes in the group D_4 denoted by $E = \{\mathsf{e}\}, C_4 = \{\mathsf{C}_4, \mathsf{C}_4^3\}, C_2 = \{\mathsf{C}_4^2\}, C_2' = \{\sigma_v^{xy}, \sigma_v^{yx}\}, C_2'' = \{\sigma_v^x, \sigma_v^y\}$. The character table for this symmetry group is given in Table S1.

We have five irreps, which we denote by m_α for $\alpha = 1-5$. Then the vector representation of the irreps is a direct sum of the irreps $\mathcal{M} = \bigoplus_\alpha d_\alpha m_\alpha$ with d_α giving the number of times the α-*th* irrep appears in the sum. d_α is calculated from orthogonality relation with the characters: $\chi_{m_\alpha}(C_k), \chi_{\mathcal{M}}(C_k)$ of the 24-dimensional representations $m_\alpha(C_k)$, $\mathcal{M}(C_k)$ respectively, for each conjugacy class C_k, where k runs over the five conjugacy classes:

$$d_\alpha = \frac{1}{h}\sum_k N_k \chi_{m_\alpha}(C_k)\bar{\chi}_{\mathcal{M}}(C_k) \tag{11}$$

where $h = 8$ is the order of the group $\mathbf{D}_4$, and N_k is the number of elements in C_k conjugacy class. The values of d_α are given in the second column in Table S1.

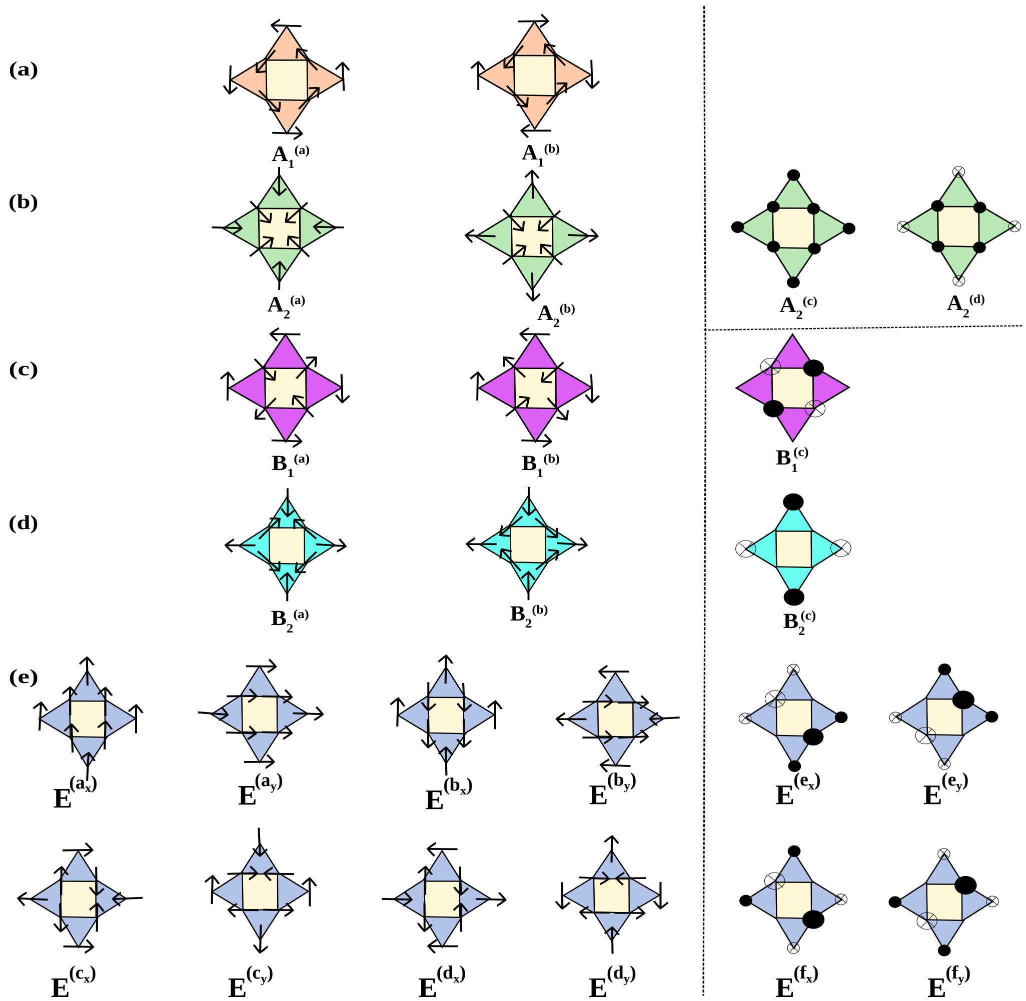

FIG. S1. We plot all the irreps' basis functions. The verticle dashed line demarcates the out-of-plane irreps m_z on the right-hand side, among which only the top row satisfies the local constraint while the others do not. The horizontal arrows dive the spin direction for $S_i^{\perp}$, while the filled and open dots correspond to S_i^z. The size of the dots corresponds to $|S_i^z|$. For $\mathsf{A}_2^{(\mathrm{c,d})}$, the size of the dots is adjusted for $|S_i^z| = 1$, while for $\mathsf{B}_{1,2}^{(\mathrm{c})}$, sites with symbols give $|S_i^z| = \sqrt{2}$, while sites without symbols have $|S_i| = 1$. Similar consideration is used for the E irreps that do not meet the local constraint.

The final task in this section is to find the basis functions $\mathcal{V}_\alpha$ of each irrep. We denote the basis vectors as $|\mathcal{V}_\alpha^\mu\rangle$, where $\alpha = 1$ for one-dimensional irreps, and $\mu = 1, 2$ (which are relabelled as x, y in Fig. S1) for the two-dimensional irrep E. The basis vectors follow a relation : $\mathcal{D}(\mathsf{g})|\mathcal{V}_\alpha^\mu\rangle = \sum_{\mu'}(U_\alpha(\mathsf{g}))_{\mu\mu'}|\mathcal{V}_\alpha^{\mu'}\rangle$, $\forall \mathsf{g}$. $(U_\alpha(\mathsf{g}))_{\mu\mu'}$ are the $\mu\times\mu$-matrix for the μ-dimensional irrep α defined for the group element g. For the one-dimensional irreps $\mathsf{A}_{1,2}$ and $\mathsf{B}_{1,2}$, $U_\alpha(\mathsf{g})$ simply gives the character of the group, and then $|\mathcal{V}_\alpha^\mu\rangle$ are the simultaneous eigenvectors of the group elements with the character being the eigenvalue. They can be solved easily and the corresponding basis functions for the one-dimensional irreps are shown in Fig. S1(a-d). For the two-dimensional E irrep, the orthogonal condition of the basis vector simplifies the above equation to $(U_\alpha(\mathsf{g}))_{\mu\mu'} = \langle\mathcal{V}_\alpha^\mu|\mathcal{D}(\mathsf{g})|\mathcal{V}_\alpha^{\mu'}\rangle$. We solve this matrix for the E irrep for each group elements, which comes out to be $U_{\mathsf{E}}(\mathsf{e}) = \mathbb{I}_{2\times2}$, $U_{\mathsf{E}}(\mathsf{C}_4) = -i\tau_y$, $U_{\mathsf{E}}(\mathsf{C}_4^2) = -\mathbb{I}_{2\times2}$, $U_{\mathsf{E}}(\mathsf{C}_4^3) = i\tau_y$, $U_{\mathsf{E}}(\sigma_v^x) = \tau_z$, $U_{\mathsf{E}}(\sigma_v^y) = -tau_z$, $U_{\mathsf{E}}(\sigma_v^{xy}) = \tau_x$, $U_{\mathsf{E}}(\sigma_v^{yx}) = -\tau_x$. τ_μ are the 2×2 Pauli matrices.

We have the multiplets as $d_\alpha = 2, 4, 3, 3$ for the four one-dimensional irreps A_1, A_2, B_1, B_2, giving 12 basis vectors, while the two-dimensional irrep with multiplicity $d_{\mathsf{E}} = 6$ gives another 12 basis vectors, as shown in Fig. S1(e). Among them, sixteen are in-plane, defined in the set $\mathsf{m}_\perp$, and eight are out-of-plane, defined in the set m_z in the main text. Among them, six out-of-plane irreps do not satisfy the local constraint of $S = 1$ per site.

XXZ and DM interactions

In the plaquette Hamiltonian, after substituting $\mathcal{S}_p = \sum_{\alpha=1}^{3n} m_\alpha \mathcal{V}_\alpha$, we obtain a Hamiltonian that is block diagonal between the irreps but contains cross-terms along the multiplicity within an irrep. So we define a d_α-dimensional spinor field for each irrep as $\boldsymbol{m}_\alpha := (m_\alpha^{(1)} \ ... \ m_\alpha^{(d_\alpha)})^T \in \mathsf{O}_p(d_\alpha)$, in which the plaquette Hamiltonian splits as

$$H_p = \sum_{\alpha=1}^{5} \boldsymbol{m}_\alpha^T \mathcal{H}_\alpha \boldsymbol{m}_\alpha, \tag{12}$$

where we have suppressed the plaquette index on the right-hand side. $\mathcal{H}_\alpha$ is a $d_\alpha \times d_\alpha$ matrix. The $\mathsf{O}_p(d_\alpha)$ symmetry of each irrep breaks into $\mathsf{O}_p(2)$ and Z_2 symmetry as follows.

For $\alpha = 1$, the A_1 irrep with $d_1 = 2$ multiplets follows an $\mathsf{O}_p(2)$ symmetry.

For $\alpha = 2$, the A_2 irrep with $d_2 = 4$, we have an emergent $\mathsf{O}_p(2) \times \mathsf{O}_p(2)$ symmetry among the multiplets, giving $\mathcal{H}_{\mathsf{A}_2} = \mathcal{H}_{\mathsf{A}_2^{(\mathrm{a,b})}} \oplus \mathcal{H}_{\mathsf{A}_2^{(\mathrm{c,d})}}$. This is obvious because $\mathsf{A}_2^{(\mathrm{a,b})}$ consists of coplanar spins while $\mathsf{A}_2^{(\mathrm{c,d})}$ are the two out-of-plane spins.

For both $\alpha = 3, d$, the $\mathsf{B}_{1,2}$ irreps with $d_{3,4} = 3$, we have an emergent $\mathsf{O}_p(2) \times \mathsf{Z}_2$ symmetry with $\mathcal{H}_{\mathsf{B}_{1,2}} = \mathcal{H}_{\mathsf{B}_{1,2}^{(\mathrm{a,b})}} \oplus \mathcal{H}_{\mathsf{B}_{1,2}^{(\mathrm{c})}}$. Here, the $\mathsf{B}_{1,2}^{(\mathrm{a,b})}$ multiplets are coplanar spins forming $\mathsf{O}(2)$ symmetry, while $\mathsf{B}_{1,2}^{(\mathrm{c})}$ consists of out-of-plane spins that do not obey local constraints.

For $\alpha = 5$, the two-dimensional E irrep with $d_5 = 6$, each component of each multiplicity gives emergent $\mathsf{O}_p(2)$ rotation as $\mathcal{H}_{\mathsf{E}} = \mathcal{H}_{\mathsf{E}^{(\mathrm{a,b})}} \oplus \mathcal{H}_{\mathsf{E}^{(\mathrm{c,d})}} \oplus \mathcal{H}_{\mathsf{E}^{(\mathrm{e,f})}}$.

All the $\mathsf{O}_p(2)$ invariant 2×2 Hamiltonian matrices for all irreps have this general form

$$(\mathcal{H}_\alpha)_{k,k'} = \epsilon_\alpha^{(k+)} \sigma_0 + \epsilon_\alpha^{(k-)} \sigma_z + \lambda_\alpha^{(kk')} \sigma_x, \tag{13}$$

where $k, k' = 1, 2 \in$ (a,b) or (c,d) or (e,f), and $\epsilon_\alpha^{k\pm} = [\epsilon_\alpha^{(k)} \pm \epsilon_\alpha^{(k')}]/2$ and $\epsilon_\alpha^{(k)}$ is the onsite energy for the k^{th} multiplet of the α-irrep, and $\lambda_\alpha^{(kk')}$ is the 'hopping energy' between the k and k' multiples. The onsite energies of the two vortices with different helicities are $\epsilon_{\mathsf{A}_1^{(\mathrm{a})}} = \epsilon_{\mathsf{A}_2^{(\mathrm{a})}} = 2\sqrt{2} + 2(\sqrt{2} - 1)D$, $\epsilon_{\mathsf{A}_1^{(\mathrm{b})}} = \epsilon_{\mathsf{A}_2^{(\mathrm{b})}} = -2\sqrt{2} - 2(\sqrt{2} + 1)D$, while the energy cost to change the helicity angle is $\lambda_{\mathsf{A}_1^{(\mathrm{a,b})}} = \lambda_{\mathsf{A}_2^{(\mathrm{a,b})}} = -4D$. The same for the two anti-vortices are: $\epsilon_{\mathsf{B}_1^{(\mathrm{a})}} = \epsilon_{\mathsf{B}_2^{(\mathrm{a})}} = -2\sqrt{2}+2(\sqrt{2}+1)D$, $\epsilon_{\mathsf{B}_1^{(\mathrm{b})}} = \epsilon_{\mathsf{B}_2^{(\mathrm{b})}} = 2\sqrt{2}-2(\sqrt{2}-1)D$, $\lambda_{\mathsf{B}_1^{(\mathrm{a,b})}} = \lambda_{\mathsf{B}_2^{(\mathrm{a,b})}} = -4D$. The out-of-plane irreps with parallel and anti-parallel spins and spin-flip energies between them as $\epsilon_{\mathsf{A}_2^{(\mathrm{c})}} = 6\Delta$, $\epsilon_{\mathsf{A}_2^{(\mathrm{d})}} = -2\Delta$, $\lambda_{\mathsf{A}_2^{(\mathrm{c,d})}} = 4\Delta$. The two irreps with only inner and out-square out-of-plane spins have the onsite energy: $\epsilon_{\mathsf{B}_1^{(\mathrm{c})}} = \epsilon_{\mathsf{B}_2^{(\mathrm{c})}} = -4\Delta$. Each two-dimensional irreps is degenerate. The in-plane FM E irreps have the energies $\epsilon_{\mathsf{E}^{(\mathrm{a})}} = 6$, $\epsilon_{\mathsf{E}^{(\mathrm{b})}} = -2$, and their hopping energy $\epsilon_{\mathsf{E}^{(\mathrm{a,b})}} = 4$. The in-plane AFM E irreps have the energies $\epsilon_{\mathsf{E}^{(\mathrm{c})}} = 4D - 2$, $\epsilon_{\mathsf{E}^{(\mathrm{d})}} = -4D - 2$, and $\epsilon_{\mathsf{E}^{(\mathrm{c,d})}} = -4$. The two out-of-plane E irreps that do not mix have the energies $\epsilon_{\mathsf{E}^{(\mathrm{e})}} = 2\sqrt{2}$, $\epsilon_{\mathsf{E}^{(\mathrm{b})}} = -2\sqrt{2}$. All energies are multiplied with J.

The explicit form of Hamiltonian in terms of the matrix elements in the basis of the irrep order parameter is

$$H_p = \sum_{\alpha=\mathsf{A}_{1,2},\mathsf{B}_{1,2}} \sum_{k,k'} (\mathcal{H}_\alpha)_{k,k'} m_\alpha^{(k)} m_\alpha^{(k')} + \sum_{k,k'} (\mathcal{H}_{\mathsf{E}})_{k,k'} \mathbf{m}_{\mathsf{E}}^{(k)} \cdot \mathbf{m}_{\mathsf{E}}^{(k')} + \sum_{\alpha=\mathsf{B}_{1,2},k=\mathrm{c}} (\mathcal{H}_{\mathsf{E}})_{k,k} (m_\alpha^k)^2. \tag{14}$$

where k, k' =a,b for all irreps, and in addition, we have k, k' =c,d for A_2 and k, k' =c,d, and k, k' =e,f for E.

Then, for all $\mathsf{O}_p(2)$ order parameters, diagonalize the corresponding 2×2 $\mathcal{H}_\alpha$ matrices by the orthogonal transformation:

$$\begin{pmatrix} \tilde{m}_\alpha^{(k)} \\ \tilde{m}_\alpha^{(k')} \end{pmatrix} = \left[\sigma_0 \cos\phi_\alpha^{(k,k')} - i\sigma_y \sin\phi_\alpha^{(k,k')}\right] \begin{pmatrix} m_\alpha^{(k)} \\ m_\alpha^{(k')} \end{pmatrix}$$

where $\phi_\alpha^{(k,k')}$ is a fixed angle of rotation that diagonalizes the corresponding irrep multiplets. Eventually, we obtain a fully diagonal Hamiltonian as

$$H_p = \sum_{\nu=(\alpha,k=1,d_\alpha)} E_\nu |\tilde{m}_\nu|^2. \tag{15}$$

We have abandoned the α and k symbols for the irreps and multiplicity and combined them into a single symbol ν which runs from 1 to $3n$ in the eigenmodes, for simplicity. Here $E_\nu = \epsilon^+_\alpha \pm \sqrt{(\epsilon^-_\alpha)^2 + \lambda^2_\alpha}$ for each $\mathsf{O}_p(2)$ multipltes of α-irreps. Their explicit forms are

$$\begin{aligned}
E_{\nu=1,2} &= -2D \pm 2\sqrt{D^2 + (1+D)^2}, && \text{for } \alpha = \mathsf{A}_1^{(\mathrm{a,b})}, \\
E_{\nu=3,4} &= E_{\nu=1,2}, && \text{for } \alpha = \mathsf{A}_2^{(\mathrm{a,b})}, \\
E_{\nu=5,6} &= 2\Delta(1 \pm \sqrt{5}), && \text{for } \alpha = \mathsf{A}_2^{(\mathrm{c,d})}, \\
E_{\nu=7,8} &= 2D \pm 2\sqrt{D^2 + 2(1-D)^2}, && \text{for } \alpha = \mathsf{B}_1^{(\mathrm{a,b})}, \\
E_{\nu=9} &= -4\Delta, && \text{for } \alpha = \mathsf{B}_1^{(\mathrm{c})}, \\
E_{\nu=10-12} &= E_{\nu=7-9} && \text{for } \alpha = \mathsf{B}_2^{(\mathrm{a,b,c})}, \\
E_{\nu=13,14} &= 2 \pm 2\sqrt{5}, && \text{for } \alpha = \mathsf{E}^{(\mathrm{a,b})}, \\
E_{\nu=15,16} &= -2 \pm 2\sqrt{1+4D^2}, && \text{for } \alpha = \mathsf{E}^{(\mathrm{c,d})}, \\
E_{\nu=17,18} &= \pm 2\sqrt{2}\Delta && \text{for } \alpha = \mathsf{E}^{(\mathrm{e,f})}.
\end{aligned} \tag{16}$$

All the energies are defined with respect to J. The values of the angle ϕ are:

$$\begin{aligned}
\phi_{\mathsf{A}_1^{(\mathrm{a,b})}} &= \frac{1}{2}\tan^{-1}\left(\frac{D}{\sqrt{2}(1+D)}\right), \quad \phi_{\mathsf{A}_2^{(\mathrm{a,b})}} = \phi_{\mathsf{A}_1^{(\mathrm{a,b})}}, \quad \phi_{\mathsf{A}_1^{(\mathrm{c,d})}} = -\frac{1}{2}\tan^{-1}\left(\frac{1}{2}\right), \\
\phi_{\mathsf{B}_1^{(\mathrm{a,b})}} &= \frac{1}{2}\tan^{-1}\left(\frac{D}{\sqrt{2}(1-D)}\right), \quad \phi_{\mathsf{B}_2^{(\mathrm{a,b})}} = \frac{1}{2}\tan^{-1}\left(\frac{-D}{\sqrt{2}(1-D)}\right), \\
\phi_{\mathsf{E}^{(\mathrm{a,b})}} &= -\frac{1}{2}\tan^{-1}\left(\frac{1}{2}\right), \quad \phi_{\mathsf{E}^{(\mathrm{c,d})}} = \frac{1}{2}\tan^{-1}\left(\frac{1}{2D}\right).
\end{aligned} \tag{17}$$

DETAILS OF CLASSICAL MONTE CARLO

In the classical Monte Carlo calculation, the final temperature is achieved by annealing from the high temperature at each step with 8×10^5 Monte Carlo steps. The expectation values of the observables are calculated by taking the average over the last 7×10^5 configurations of a total 8×10^5 Monte Carlo steps with system size $N = 6L^2$, with L number of unit cells. All the static structure factor averages are performed over system size, $L = 20$ at temperature 10^{-3}. The position vectors of each sublattice (denoted with indices 0,1, ... in Fig. 1(a) of main text) are taken as considering the origin at the center of the square,

$$\delta_0 = \left(\frac{-1}{4}, \frac{-1}{4}\right), \quad \delta_1 = \left(\frac{1}{4}, \frac{-1}{4}\right), \quad \delta_2 = \left(\frac{1}{4}, \frac{1}{4}\right), \quad \delta_3 = \left(\frac{-1}{4}, \frac{1}{4}\right), \quad \delta_4 = \left(0, \frac{-1}{2}\right), \quad \delta_5 = \left(\frac{1}{2}, 0\right) \tag{18}$$

STRUCTURE FACTOR PLOTS

In this section, we list the real space spin configurations of all the phases and their respective structure factors. As defined in the main text, the different structure factors are

$$\begin{aligned}
\chi(\mathbf{k}) &= 1/\mathcal{N}\sum_{i,j}\langle \mathbf{S}_i \cdot \mathbf{S}_j\rangle \exp\left(\mathrm{i}\mathbf{k}\cdot(\mathbf{r}_i - \mathbf{r}_j)\right) \\
\chi^\perp(\mathbf{k}) &= 1/\mathcal{N}\sum_{i,j}\langle \mathbf{S}_i^\perp \mathbf{S}_j^\perp\rangle \exp\left(\mathrm{i}\mathbf{k}\cdot(\mathbf{r}_i - \mathbf{r}_j)\right) \\
\chi^z(\mathbf{k}) &= 1/\mathcal{N}\sum_{i,j}\langle \mathbf{S}_i^z \mathbf{S}_j^z\rangle \exp\left(\mathrm{i}\mathbf{k}\cdot(\mathbf{r}_i - \mathbf{r}_j)\right)
\end{aligned} \tag{19}$$

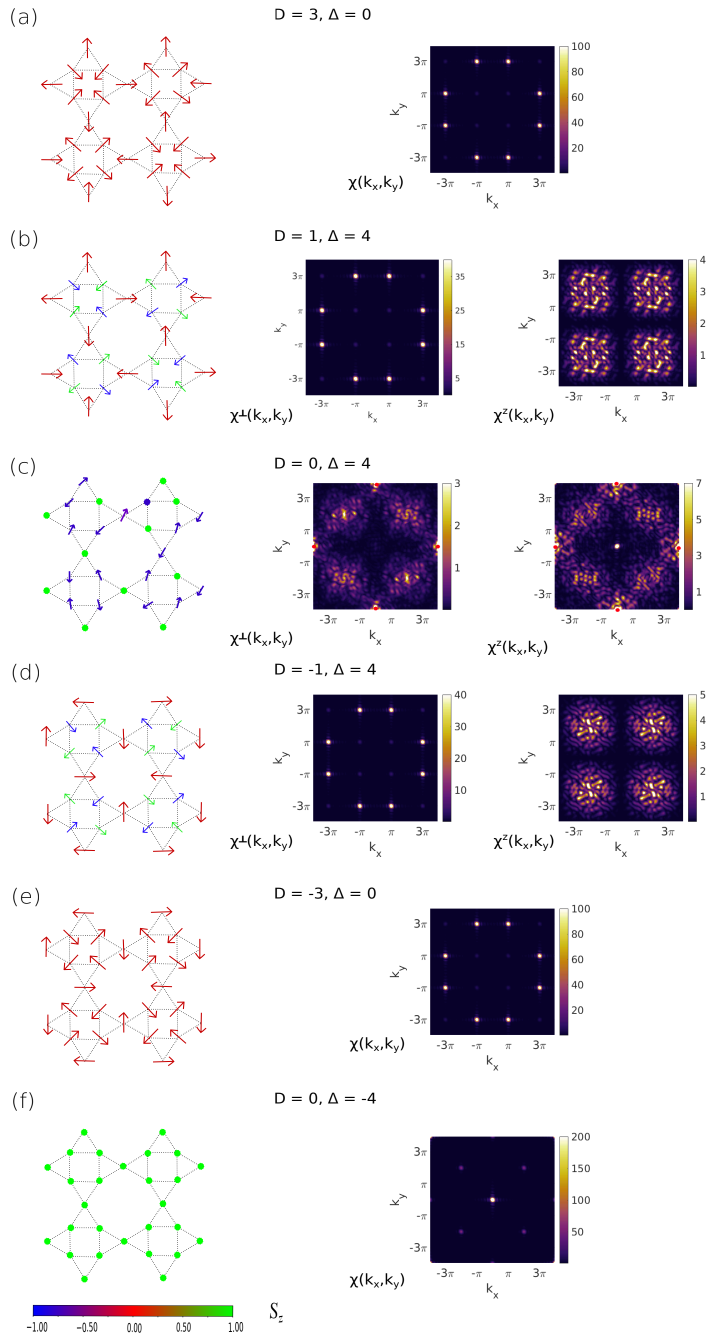

FIG. S2. The real spin configurations (left panel) and the corresponding structure factor (right panel) are plotted for various phases for the AFM coupling $J = +1$. (a) Order phase (red region in the phase diagram) with staggered anti-vortices between the neighboring sites, showing Bragg-like peaks at a finite but preferential wavevector. (b) Mixed or fragmented phase where the inner anti-vortices turn into an AFM-anti-vortex with opposite S_i^z components, while $S_i^z = 0$ for the outer anti-vortex. The S_i^z values, however, take random values and show disorder features in the corresponding structure factor without any pinch-point correlation. This is expected as the inner vortices become decoupled from each other, lacking any significant correlation between them. (c) A CSL phase (close to the Z_2 CSL phase) showing larger spectral weight the S_i^z correlation function with pinch-points. (d) The mixed or fragmented phase for $D < 0$ which is similar to the mixed phase for $D > 0$ except here vortices replace the anti-vortices. (e) Orderd phase for D<0, similar to the $D > 0$ case in (a), with vortices replacing anti-vortices. (f) A collinear out-of-plane FM phase arising in the limit of strong our-of-plane anisotropy term $\Delta \to -\infty$.

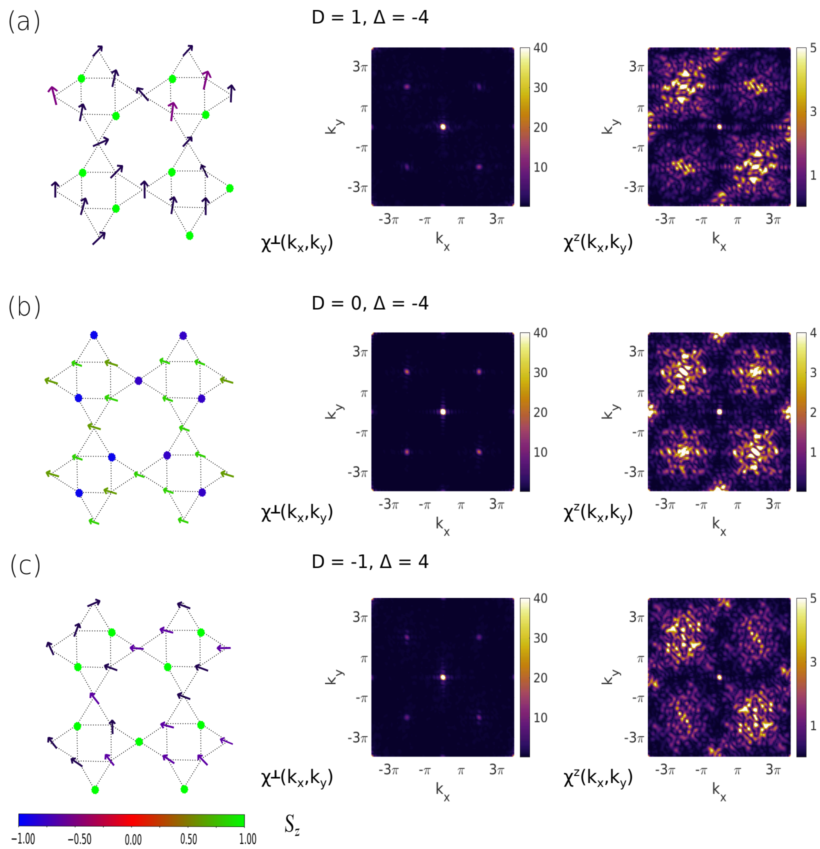

FIG. S3. Similar to Fig. S2, but for the FM interaction $J = -1$. All three phases shown here are the fragmented phases at different values of D, and Δ, showing pinch-point in the S_i^z correlation function, but FM ordering in the in-plane component.

SOFT-SPIN APPROXIMATION

In this section, we analyze the Hamiltonian in Eq. 4 with 'soft spin' approximation i.e. spin length constraint ($|\mathbf{S}_i|^2 = 1$) is softened from exact value of 1 per site to the global value of $\sum_i^N |\mathbf{S}_i|^2 = NS$. Because of the global constraint, we have a uniform (fixed) chemical potential (Lagrangian multiplier) in the theory. Then, following Ref. 25, we have diagonalized the Hamiltonian in the Fourier space of the spin. There, a spin vector is defined per unit cell, not in the plaquette, which means we have six sublattices as $\mathcal{S}_i$=(S_0^x, S_0^y, S_0^z, S_1^x, ..., S_5^z). We Fourier transform the spin vector as $\mathcal{S}(\mathbf{q}) = \frac{1}{\sqrt{N}} \sum_i \mathcal{S}_i e^{-i\mathbf{q}\cdot\mathbf{r}_i}$, where $\mathbf{r} = a\mathbf{n}_1 + b\mathbf{n}_2$ with integers a, b and unit vectors $\mathbf{n}_1 = (1,0), \mathbf{n}_2 = (0,1)$. The Hamiltonian is then diagonal in the momentum space as

$$H = \sum_{\mathbf{q}} \mathcal{S}^T(\mathbf{q})^T \mathcal{H}(\mathbf{q}) \mathcal{S}(\mathbf{q}), \tag{20}$$

where $\mathcal{H}(\mathbf{q})$ is a 18×18 matrix. We can now diagonalize the $\mathcal{H}(\mathbf{q})$ matrix, which gives the energy eigenvalues $E_\nu(\mathbf{q})$. The lowest energy state is the ground state, and then we plot a few low-energy excited states in Fig. S4.

We note that the analysis on the Fourier basis leads to a violation of the local constraint and hence, inconsistency is expected between the real-space model and the Fourier space one, especially in the spin liquid phase. In the CSL phase, we find an extremely flat band as the lowest energy state, suggesting extensive degeneracy as expected here. We see the flat band in all the mixed phases as well. In addition, the spectrum is gapless in both phases, with gapless points present at $(\pm\pi, \pm\pi), (\pm\pi, \pm 3\pi)$, and $(\pm 3\pi,) \pm 3\pi)$, as shown in Fig. S4. The band degeneracy, denoted with d in the spectrum at each region is different: d=4(2) for $\Delta < 1 (> 1)$, d=6 at $\Delta = 1$ in the CSL phase where D=0; and d=2 for mixed phases both for $J = +1$ and -1. Hence, there is no simple positive sum of the constrainer rule here; the direct matching of singular/non-singular bands to emergent gauge fields/fragility is not possible.

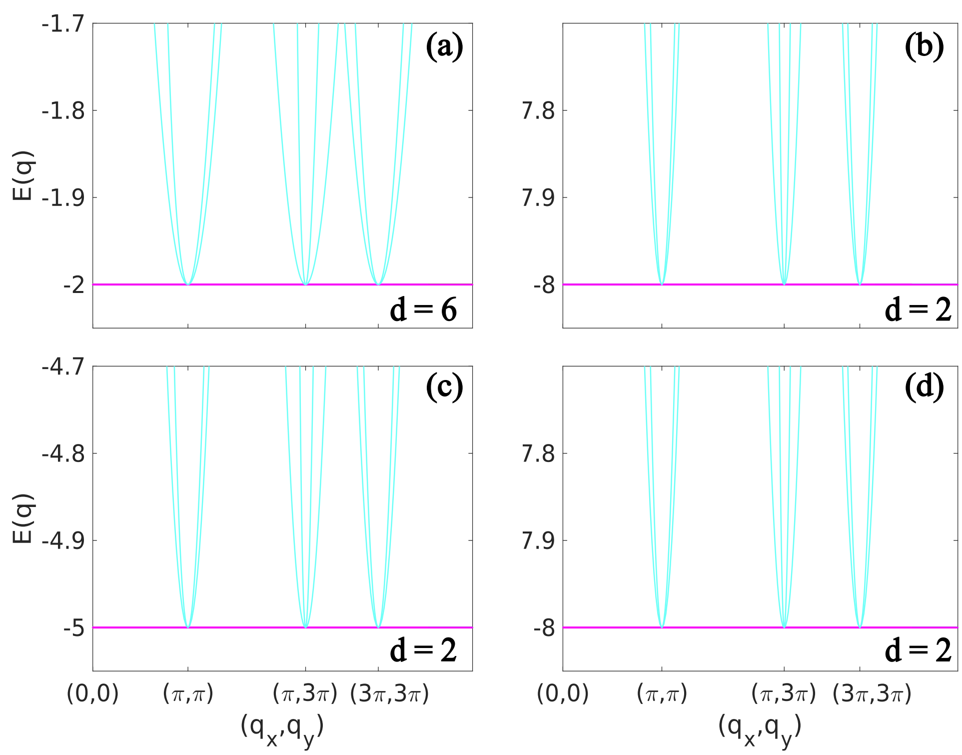

FIG. S4. Energy dispersion of the Hamiltonian $\mathcal{H}(\mathbf{q})$ at four with re)spective degeneracy of flat bands d, for (a) $\Delta = 1.0, D = 0.0$ (CSL), (b) $\Delta = 4.0, D = 1.0$ (Mixed phase) for $J = +1$ and (c) $\Delta = -2.5, D = 0.0$ (d) $\Delta = 4.0, D = 1.0$ (Mixed phases) for J = -1

As discussed rigorously in the main text, the spin liquids (cyon(/black) colored phase for J=+1(/-1)) phase has pinch points belonging to the algebraic class of CSLs with 'emergent' low-energy gauge field excitations. The mixed (black-colored phase for J=+1) phase has no pinch points and, hence, belongs to the fragile class of CSLs. All the other ordered phase regions have dispersive bands.

Finite Magnetic field

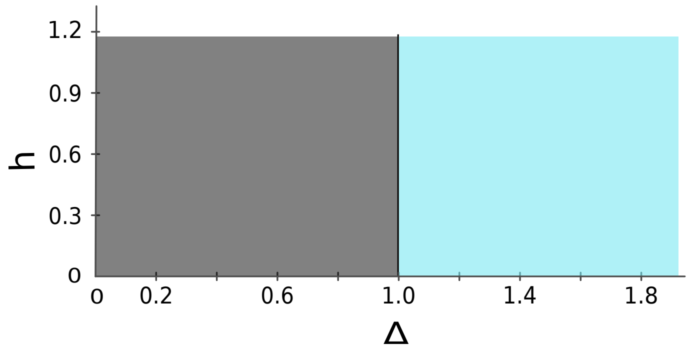

FIG. S5. Phase diagram at D=0, as a function of h and Δ. For $\Delta < 1$, the phase is a mixed phase and spin liquid for another case. The mixed phase here is unstable for any finite value of D; the phase becomes ordered in and out-of-plane for non-zero D value.

The external magnetic field is applied along the z-axis to the Hamiltonian, now written as

$$H_{mag} = H_{\mathrm{XXZ-DM}} - h \sum_i S_i^z. \tag{21}$$

The phase diagram as a function of h and Δ is presented in Fig. S5 for $D = 0$. A mixed phase of disordered in-plane spins with ordered out-of-plane components is observed at $D = 0$ for $\Delta < 1$ with increasing h. The in-plane disordered spins exhibit a coexisting Bragg-like leak at $(0, 4\pi)$, and pinch points at $(\pm\pi, \pm 3\pi)$. The ordering along the z components is FM type. This phase is unstable for any finite value of D. A finite value of D gives an ordered phase depending on the sign of the D value, where the in-plane spins form an ordered supercell structure and the out-of-plane spins are ferromagnetically ordered. As $\Delta > 1$, the spins become disordered both in in-plane and out-of-plane components. This phase also has pinch-points in the correlation function, indicating power-law correlations. This phase survives at finite values of D. Therefore, we conclude that, by applying the external magnetic field, the spin liquid phase can be stabilized in these materials.